Hindawi
Journal of Nanomaterials
Volume 2019, Article ID 7915129, 10 pages
https://doi.org/10.1155/2019/7915129

Research Article

Study on the Influencing Factors of Ultrafine Spherical RDX during Spray Drying with Low Speed

Wenzheng Xu, Jie Wang, Jinyu Peng, Xin Liang, Hao Li, and Jingyu Wang

School of Environment and Safety Engineering, North University of China, Taiyuan, 030051 Shanxi, China

Correspondence should be addressed to Wenzheng Xu; xuwznuc@126.com

Received 20 October 2018; Accepted 29 January 2019; Published 14 March 2019

Academic Editor: Domenico Acierno

Cyclotrimethylene trinitramine (RDX, $C_3H_6N_6O_6$) with the size of 400 to 600 nm was prepared by low-speed spray-drying method. Meanwhile, the crystal morphology, particle size, crystal structure, thermal decomposition properties, and impact sensitivity properties of the raw materials of RDX and the prepared ultrafine spherical RDX were characterized by scanning electron microscope (SEM), laser particle size analyzer (LPSA), X-ray diffractometer (XRD), differential scanning calorimeter (DSC), and impact sensitivity instrument. The factors affecting experimental results were discussed; the size and morphology of RDX crystals were found to be affected by drying temperature, spray speed, and RDX mass fraction in solution. The optimal preparation conditions for the ultrafine spherical RDX were studied, and the results showed that the RDX particles with the best morphology and particle uniformity were prepared when the drying temperature was 90°C, spray speed was 1 ml/min, and the RDX mass fraction in solution was 4%. As a result, the activation energy (Ea) of the ultrafine spherical RDX was lower than that of raw RDX by 24.52 KJ·mol^{-1}, and the characteristic drop (H_{50}) of the ultrafine spherical RDX was higher by 35.3 cm.

1. Introduction

Nanoscale energetic materials have various advantages, such as the following: high stability and safety, fast energy release, and high energy density [1, 2]. Ultrafine spherical energetic material crystals have the characteristics of smooth surfaces, regular shapes, and excellent fluidity. Compared with traditional energetic materials, the performance of detonation, energy release, safety, and other properties of ultrafine spherical energetic materials are higher. This series of improvements in performance had increased the power, reliability, and safety of weapon systems while more applications were developed [3, 4].

In the current study, the main methods for refining energetic materials were as follows: sol-gel methodologies [5, 6], chemical recrystallization [7–10], rapid expansion of supercritical solutions (RESS) [11–14], mechanical ball milling [15, 16], and supercritical fluid expansion technology [17–19]. The characteristic drop (H_{50}) of the RDX (cyclotrimethylene trinitramine) which was prepared by the sol-gel method by TM was twice higher than the characteristic drop of raw RDX [5]. Spherical TATB (1, 3, 5-triamino-2, 4, 6-trinitrobenzene) with a particle size of 60 nm was prepared by chemical recrystallization by Yang et al. [11] which uses the concentrated sulfuric acid as a solvent and water as a nonsolvent. Sphere RDX particles with a particle size range of 0.36 to 2.48 μm were prepared by Lee et al. [14] with the RESS process. It was known from the study that the morphology had a significant effect on the bulk density of the crystal. Nano-TATB with the average particles size of 58.1 nm was prepared by high-energy mechanical milling method by Song et al. [15]. The RDX with a particle size of 500 nm was prepared by the supercritical fluid expansion technology by Qiu et al., which showed that the shock wave sensitivity and impact sensitivity were lower than those of raw RDX [19].

The spray-drying [20–23] method was suitable for the preparation of heat-sensitive substances due to the stable preparation process, the convenient operation, and the products which did not need to be crushed and sieved

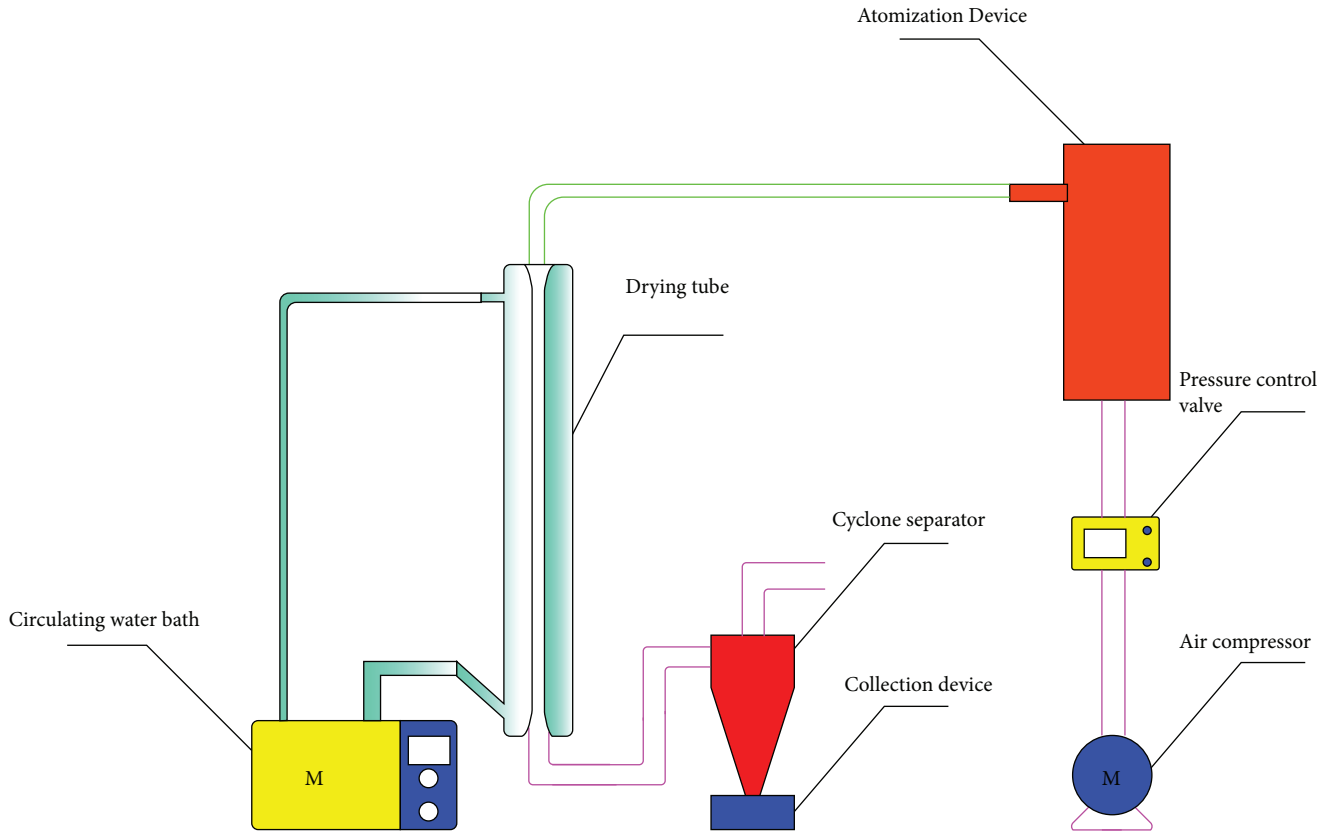

Figure 1: Experimental device for preparing ultrafine spherical RDX.

after drying. The spray-drying method was used to prepare the spherical RDX with a particle size of 0.5 μm to 4 μm by Jingyu et al. [21] with the spray speed of 10 ml/min. The measured properties were all higher than those of the raw material RDX. The spherical RDX with a particle size of 0.8 to 2.6 μm was prepared by Kim et al. [23] with ultrasonic spray, and the size of RDX crystals was found to be strongly affected by operating parameters including RDX concentration and furnace temperature.

In this paper, the ultrafine spherical RDX particles with uniform particle size were prepared by changing the process under the condition of low-speed spray, and the samples were characterized.

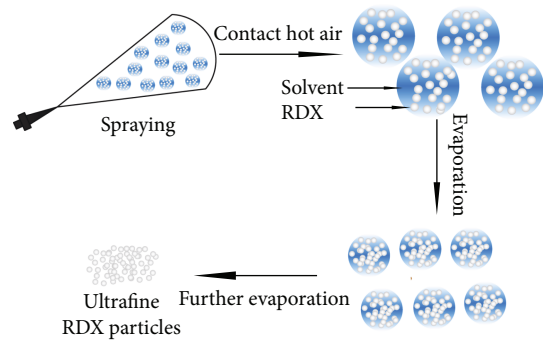

Figure 2: Schematic of the formation of ultrafine spherical RDX.

2. Experiment

2.1. Reagents and Instruments. Raw RDX with particle size of 100 μm was produced by Gansu Yinguang Chemical Industry Group Co. Ltd. Analytically pure acetone was supplied by Tianjin Shentai Chemical Reagent Co. Ltd.

The Hitachi S-4700 cold field emission scanning electron microscope (FE-SEM, Japan) was used to characterize the morphology and surface appearance of the ultrafine RDX. The BI-90PLUS Laser Particle Size Analyzer (Brookhaven Instruments Corporation) was used to test the particle size of ultrafine RDX. The DX-2700 X-ray powder diffraction system was used to characterize the crystal type of the crystal. Testing conditions included a target material (Cu) with tube voltage of 40 kV, tube current of 30 mA, a 5° start angle, and a 50° end angle. The DSC-131 differential scanning calorimeter was used to characterize the thermal decomposition ability. In the test, each 0.7 mg sample was placed in a closed aluminum crucible with 30 μl volume and a hole in the lid. Samples were measured with a temperature profile of 30°C to 300°C with heating rate of 5, 10, 15, and 20°C/min in nitrogen atmosphere and flow of 30 ml/min. An ERL Type 12 drop hammer apparatus was used to conduct impact sensitivity tests according to GJB-772A-97 standard method 601.3. Testing conditions consisted of a drop weight of 5.00 ± 0.002 kg, sample mass of 35 ± 1 mg, and relative

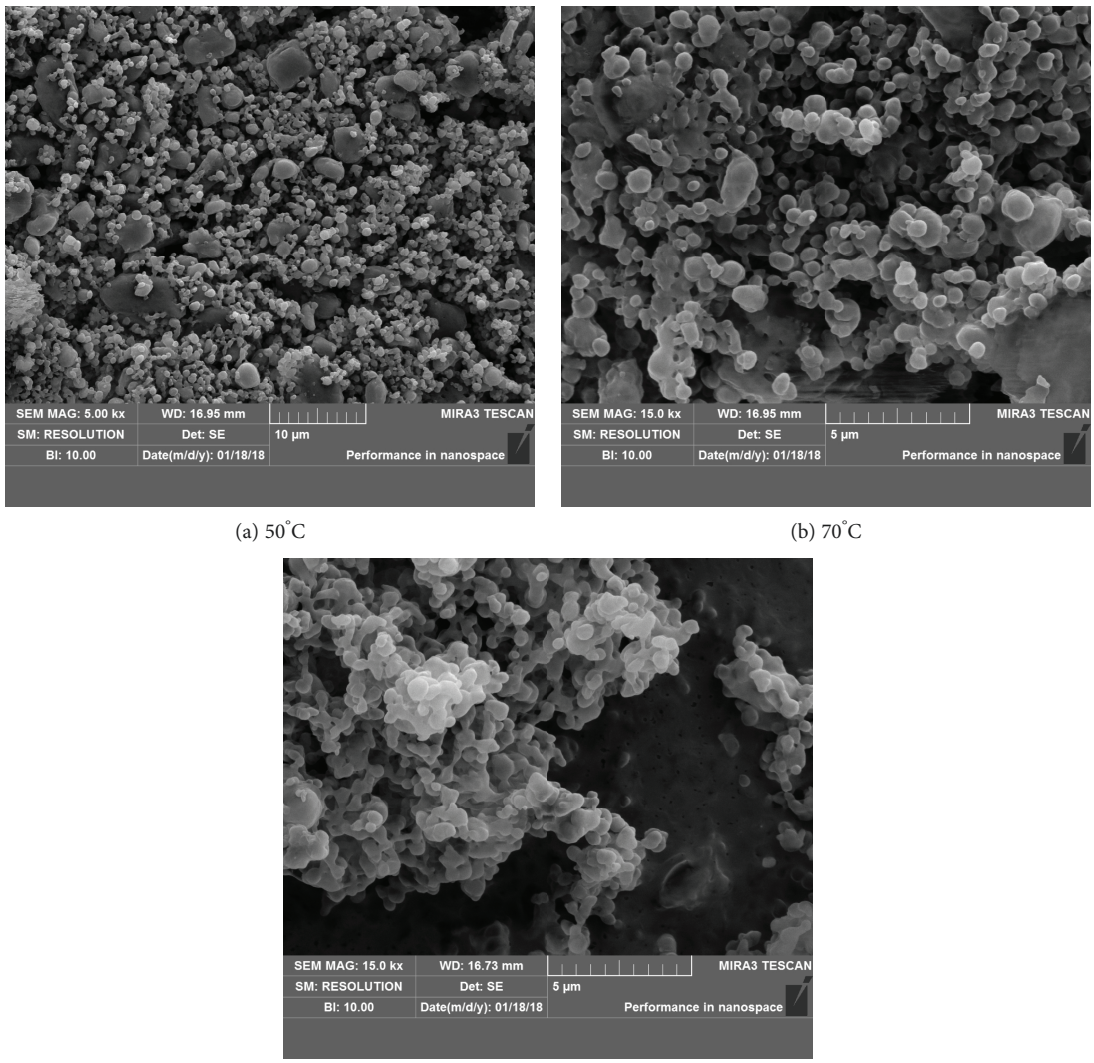

(a) 50°C

(b) 70°C

(c) 90°C

Figure 3: RDX samples prepared at different drying temperatures.

Table 1: Spraying speed and spraying pressure.

Spraying speed (ml/min)	0.625	1	1.93
Spraying pressure (Mpa)	0.05	0.2	0.4

humidity of 50%. Test results were represented by a critical drop height of 50% explosion probability (H_{50}).

2.2. Experimental Principle

2.2.1. Experiment Procedure. The process of spray-drying refinement to prepare the ultrafine spherical RDX is shown in Figure 1. The experimental process was as follows: Firstly, a certain amount of raw RDX was dissolved in acetone and stirred at room temperature until completely dissolved. Secondly, the dissolved RDX solution was poured into the atomizer device. Meanwhile, the air compressor and the pressure control valve were turned on, and the input air pressure of the air compressor was adjusted. Then, the droplets of RDX solution were formed and sprayed from the spray device. When the droplets passed through the drying tube, the acetone evaporated rapidly due to the high temperature. Finally, ultraspherical RDX was collected in the collection device after passing through the cyclone separator.

2.2.2. Particle Formation during Spray and Drying. It was assumed that the particles was formed under the following ideal conditions:

(1) The tiny droplets were considered to be approximately spherical which were sprayed, and the crystallized RDX particles were also considered to be spherical

(2) During the crystallization process, the RDX in the tiny droplets was completely precipitated and the RDX was not carried away with the volatilization of

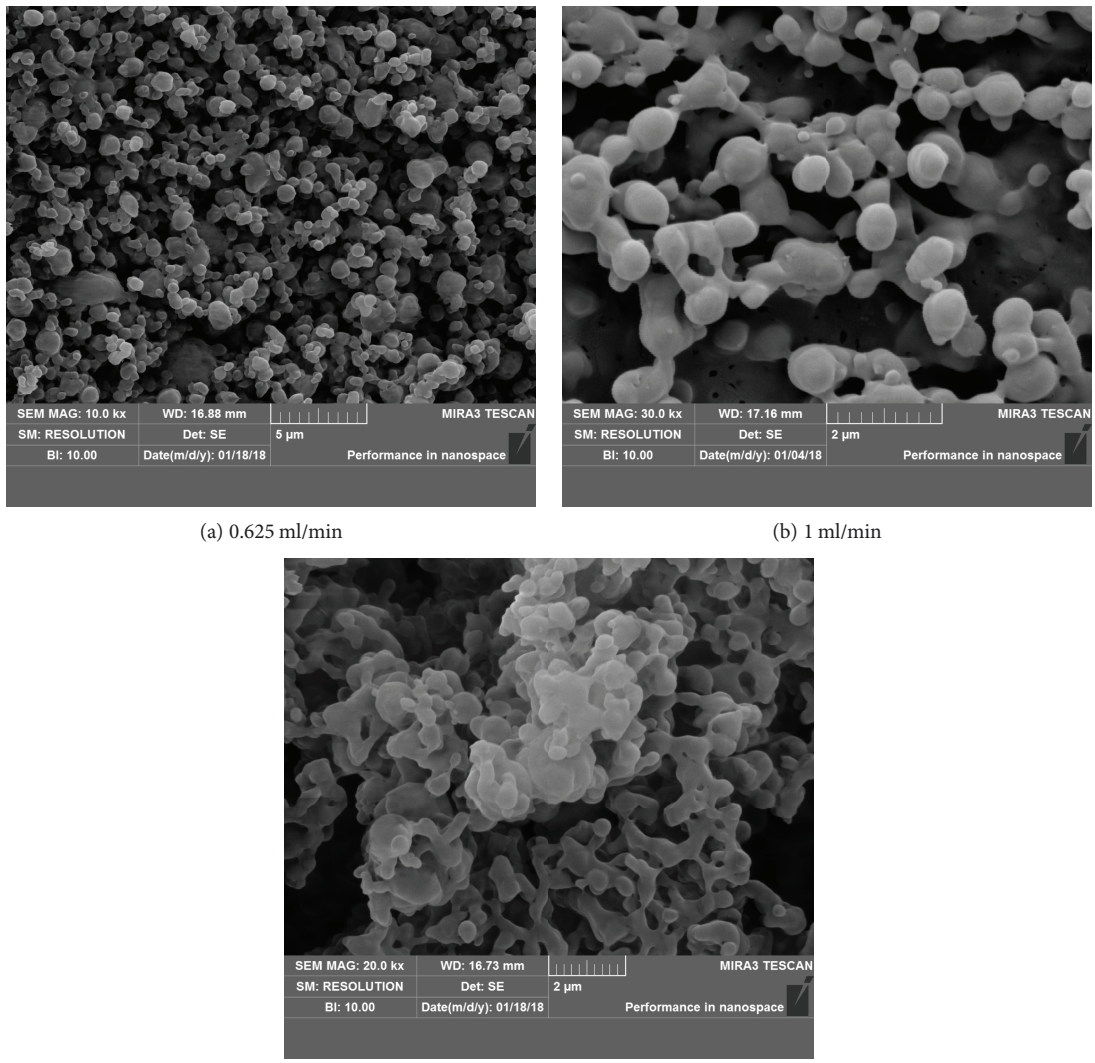

(a) 0.625 ml/min

(b) 1 ml/min

(c) 1.93 ml/min

Figure 4: RDX samples prepared under different spray speeds.

the solvent; that is, the crystallization rate of the explosives was 100%.

(3) The volatilization of the solvent and the crystallization of RDX were instantaneously completed. In the process, the crystals grew within the droplets, which rarely collided and associated with each other

The relationship between the droplet size and the final particle size could be established:

$$M_1 = \frac{\pi C D^3}{6}, \qquad M_2 = \frac{\pi \rho d^3}{6}, \tag{1}$$

where D is the diameter of a droplet and C is the concentration of the solution, M_1 is the mass of the explosive particles before the reaction, M_2 is the mass of the explosive particles after the reaction, d is the droplet crystallizing after the reaction, and ρ is the crystal density of the explosive.

According to the assumptions, the mass of the explosive does not change during the reaction ($M_1 = M_2$). The relationship between the diameter of the droplets and that of the explosive particles can be obtained from the above equations:

$$d = D\left(\frac{C}{\rho}\right)^{1/3}. \tag{2}$$

It can be seen that the particle size of the explosive particles is determined by the droplet diameter and the solution concentration. And the influence of the droplet diameter is greater than that of the concentration of the solution. Therefore, the spray condition and the particle size of droplets are the keys to preparing the ultrafine spherical particles.

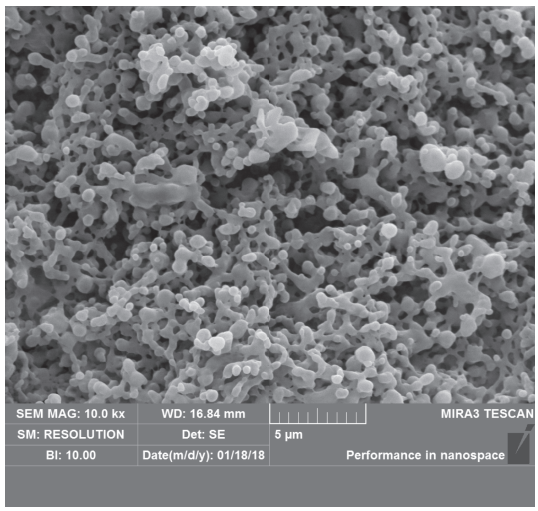

(a) 2 wt%

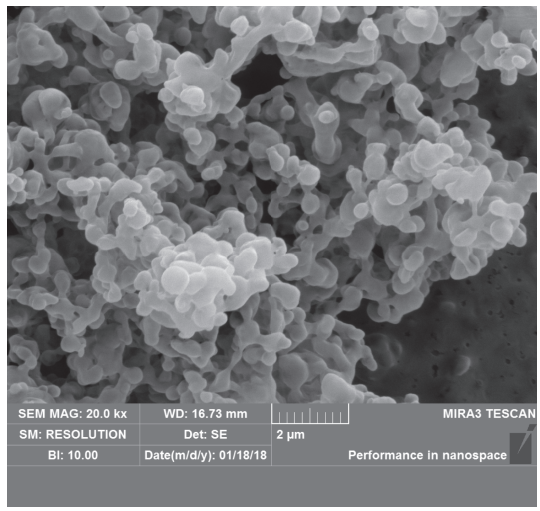

(b) 4 wt%

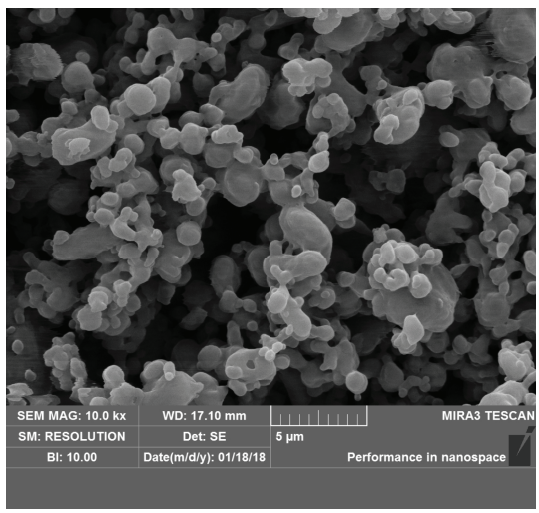

(c) 8 wt%

Figure 5: RDX samples prepared from different RDX mass fractions.

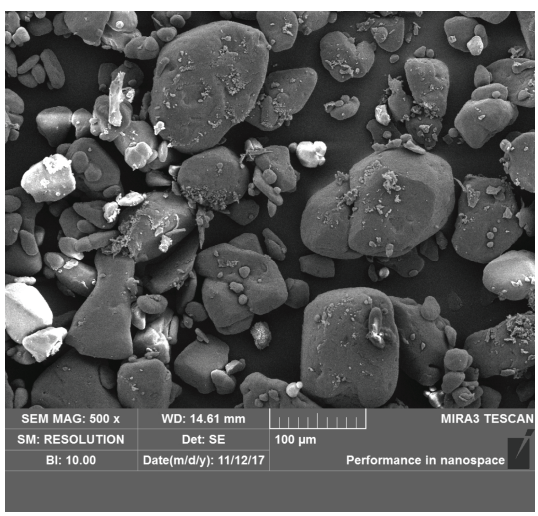

(a) Raw RDX

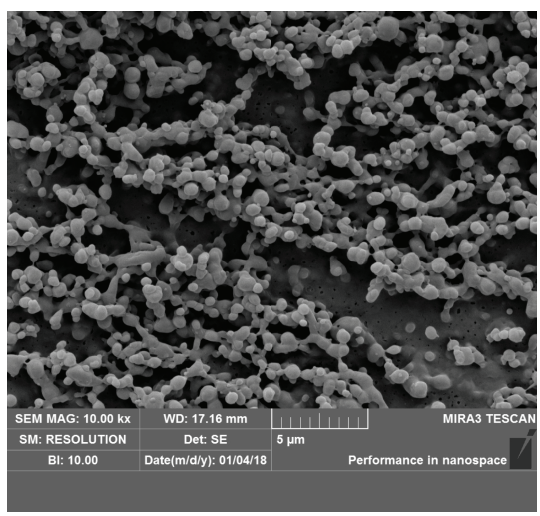

(b) Ultrafine spherical RDX

Figure 6: SEM images of raw RDX and ultrafine spherical RDX.

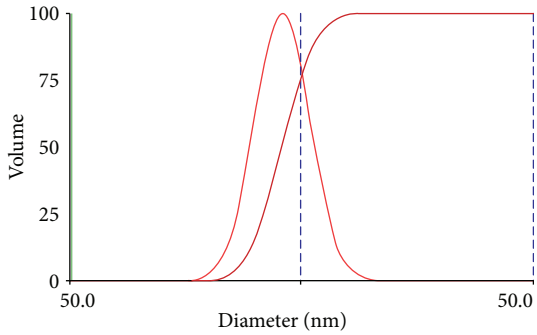

Figure 7: Particle size distribution curve of ultrafine spherical RDX.

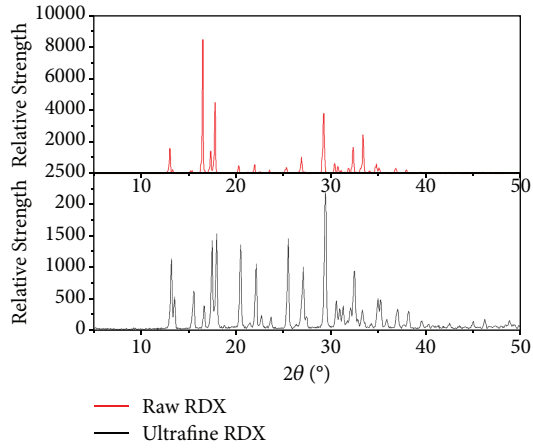

Figure 8: X-ray diffraction patterns of raw material RDX and the ultrafine spherical RDX.

The crystallization process of RDX during spray drying is shown in Figure 2.

3. Results and Discussion

3.1. Effect of Different Factors on Crystal Morphology

3.1.1. Effect of Different Temperatures on the Crystal Morphology of RDX. When the spraying speed was 1 ml/min and the mass fraction of RDX in the solution was 4%, the ultrafine RDX particles were prepared at various drying temperatures (50°C, 70°C, and 90°C), which are shown in Figure 3. When the drying temperature was 50°C (Figure 3(a)), the RDX particles were generally larger with irregular shapes and the size of particles was not uniform. When the drying temperature was 70°C (Figure 3(b)), some large-size RDX particles were obtained but significantly less than those at 50°C and the shapes of the RDX particles were regularly spherical and ellipsoid. When the drying temperature was 90°C (Figure 3(c)), the average size of RDX particles was 500 nm and the particle size distribution was narrower. At this time, the shapes of the RDX particles were spherical.

The results showed that the best drying temperature for the experiment was 90°C. At this temperature, the obtained RDX had the best morphology and the size of the particles was uniform. The reason was that the evaporation rate of the solvent increased with the increasing of the drying temperature and the RDX particles dried out when the solution droplets had not yet agglomerated. Therefore, the obtained RDX particles with a small particle size were uniform and spherical. When the drying temperature was lower, some parts of the solution droplets agglomerated without instantaneous drying, the size of the obtained RDX particles was nonuniform and large. The result showed that the drying temperature was an important factor affecting the shape and size of the RDX particles. Considering the safety of the experiment, 90°C was the highest temperature that could be set for this experiment due to the fact that air was used as the drying medium in this experiment.

3.1.2. Effect of Different Spraying Speeds on the Crystal Morphology of RDX. In this experiment, we controlled the spraying speed by controlling the spraying pressure. The comparison between the two is shown in Table 1.

When the drying temperature was 90°C and the mass fraction of RDX in the solution was 4%, the ultrafine RDX particles were prepared in the various spraying speed conditions (0.625 ml/min, 1 ml/min, and 1.93 ml/min), which are shown in Figure 4. When the spraying speed was 0.625 ml/min (Figure 4(a)), more RDX particles with irregular shapes and large size were formed. When the spraying speed was 1 ml/min (Figure 4(b)), the size of RDX particles obtained was uniform and the shape was spherical. When the spraying speed was 1.93 ml/min (Figure 4(c)), obvious agglomeration was observed among the RDX particles and some of the agglomerated large-size RDX particles were obtained. The reason was as follows: when the spraying pressure was too much, the gas flow rate was high and the pressure on the droplets was increased which caused adjacent droplets to agglomerate. Meanwhile, the RDX droplets entered the collection device when they passed through the drying tube due to the high gas flow rate. Under the erosion of the unevaporated solvent, some of the RDX particles were stuck. When the spray pressure was too low, the spray effect was poor, resulting in larger droplets which formed the RDX particles with a larger size after drying. Thus, 0.2 Mpa was the best spraying pressure and 1 ml/min was the best spraying speed in the experiment.

3.1.3. Effect of Different RDX Mass Fractions on the Crystal Morphology of RDX. When the drying temperature was 90°C and the spraying speed was 1 ml/min, the ultrafine RDX particles were prepared at various RDX mass fractions in the solution, which are shown in Figure 5. It could be observed from Figure 5(a) that the particle size uniformity was poor and there was an adhesion phenomenon when the mass fraction of RDX was 2.0 wt%. Figure 5(b) showed that the RDX particles with a high size uniformity and a spherical shape were obtained when the mass fraction of RDX was 4.0 wt%. When the mass fraction of RDX was 8.0 wt% (Figure 5(c)), the RDX particles with irregular shapes and larger size were obtained. The reason of those results was as follows: when the RDX mass fraction in the solution was

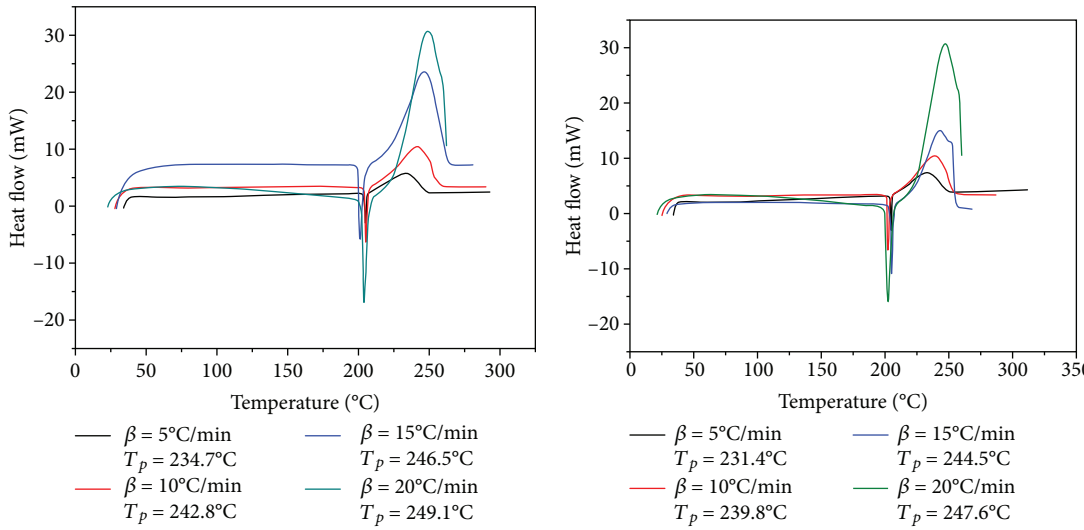

(a) Raw RDX (b) Ultrafine spherical RDX

Figure 9: DSC curves of raw RDX and the ultrafine spherical RDX.

too large, the content of the RDX in each droplet after the spray was much higher and the RDX particles obtained after drying were larger in size and irregular in shape. When the RDX mass fraction in the solution was too low, the RDX particles were eroded more easily by the excess solvent after drying. Therefore, 4 wt% RDX/acetone was the best RDX mass fraction in the solution for this experiment.

Raw RDX (Figure 6(a)) and the ultrafine spherical RDX (Figure 6(b)) (drying temperature 90°C, spraying speed 1 ml/min, and mass fraction of explosive solution 4%) are shown in Figure 6.

3.2. Particle Size Analysis. Under the optimum conditions (drying temperature of 90°C, spray speed of 1 ml/min, and RDX mass fraction in solution of 4%), the particle size distribution of ultrafine spherical RDX particles was characterized, as shown in Figure 7.

As shown in Figure 7, the median diameter of the ultrafine spherical RDX was 517 nm, and the particle size distribution was narrow. Meanwhile, it could be seen from Figure 6(b) that the ultrafine spherical RDX prepared had a particle size range of 400-600 nm, an obvious spheronization effect, and a smooth surface.

3.3. Crystal Analysis. The XRD patterns of raw RDX and the ultrafine spherical RDX prepared by spray drying are shown in Figure 8.

It could be seen that the resulting diffraction angle and peak of the ultrafine spherical RDX could be mapped to those of the diffraction pattern of raw RDX, which indicated that the crystal type of ultrafine RDX was α-type. The peak value of the ultrafine spherical RDX was lower than that of raw RDX, and the shape of the peak was broadened, which concluded that the particle size of RDX had been significantly reduced after refinement.

3.4. Thermal Performance Analysis. At the heating rate β of 5°C/min, 10°C/min, 15°C/min, and 20°C/min, the thermal ability of raw RDX (Figure 9(a)) and the ultrafine spherical RDX (Figure 9(b)) prepared by spray drying were tested and the results are shown in Figure 9.

It could be observed that the DSC curves of the ultrafine spherical RDX prepared by spray drying were basically consistent with those of raw RDX. For the same heating rate, the decomposition peak temperature of ultrafine spherical RDX was slightly lower than that of raw RDX. For different heating rates, the decomposition peak temperatures of raw RDX and the ultrafine spherical RDX were increased with the increase of the heating rate.

Kissinger [24] formula (3) and Rogers and Dauh [25] formula (4) were used to calculate the activation energy (Ea) and the frequency factors (A). A straight line was obtained and is shown in Figure 9 when $\ln(\beta_i/T_{pi}^2)$ was plotted against $1/T$. From the slope and the intercept of the straight line, the apparent activation energy and the preexponential factor could be calculated; the Kissinger fitting degree of raw RDX (Figure 10(a)) and the ultrafine RDX (Figure 10(b)) were more than 99%, indicating that the measurement data was accurate and reliable. The results are shown in Table 2.

$$\ln\left(\frac{\beta_i}{T_{pi}^2}\right) = \ln\left(\frac{AR}{E}\right) - \frac{E}{RT_{pi}}, \tag{3}$$

$$A = \frac{E\beta_i}{RT_{pi}^2}\exp\left(\frac{E}{RT_{pi}}\right), \tag{4}$$

where β_i is the heating rate ($K \cdot min^{-1}$), T_{pi} is the decomposition peak temperature of the explosive at heating rate β_i, A is the preexponential factors (min^{-1}), R is the gas constant ($8.314\,J \cdot mol^{-1} \cdot K^{-1}$), and E is the apparent activation energy ($J \cdot mol^{-1}$).

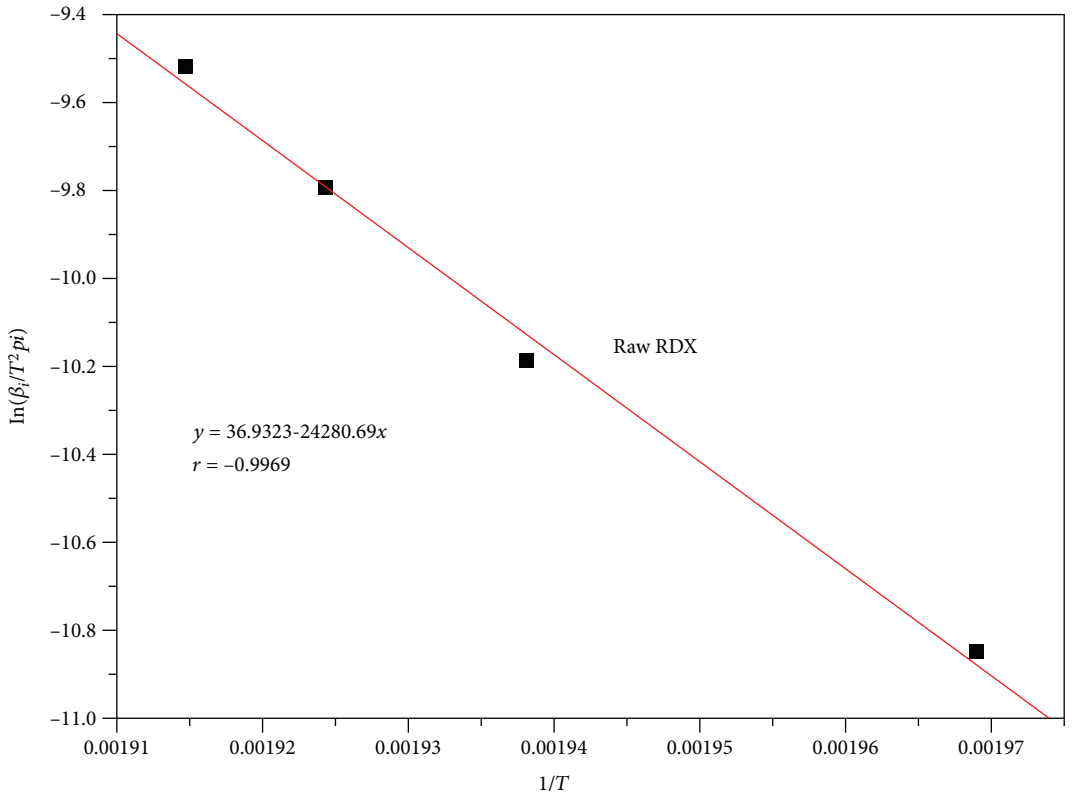

(a) Raw RDX

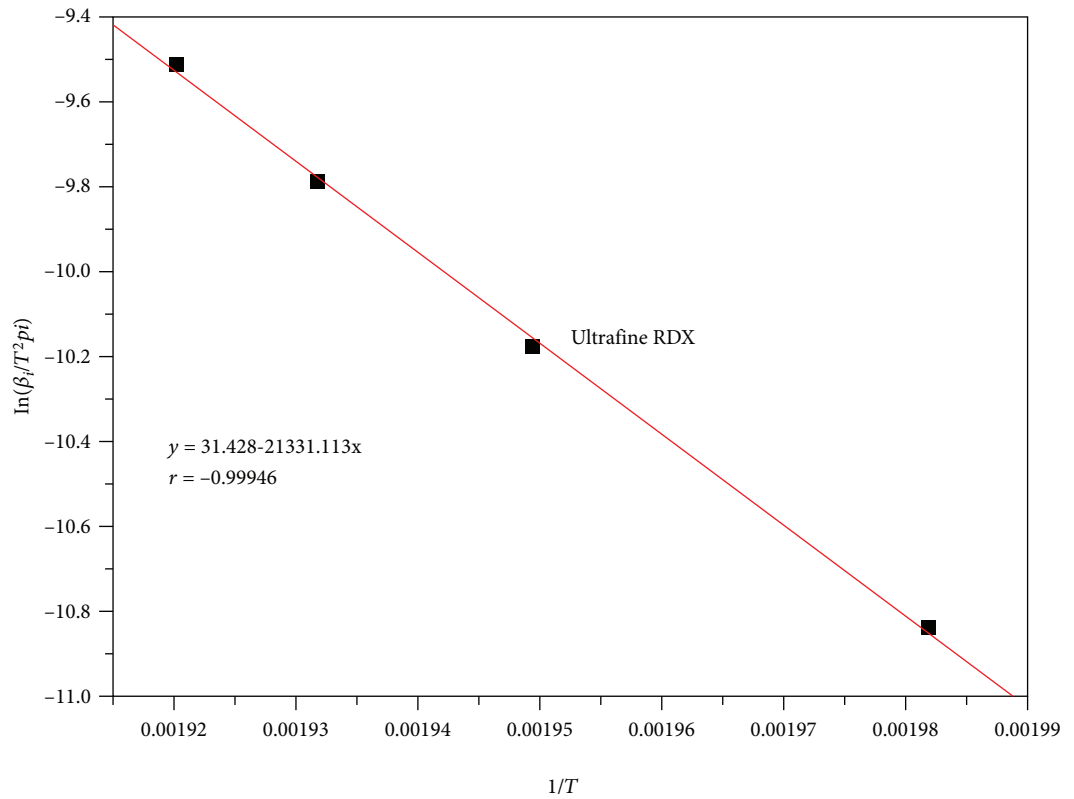

(b) Ultrafine RDX

Figure 10: The Kissinger fitting lines of raw RDX and ultrafine RDX.

Table 2: Thermal decomposition kinetics parameters of RDX and ultrafine spherical RDX.

Sample	E (KJ/mol^{-1})	A (min^{-1})	T_e0 (°C)	T_b (°C)
Raw RDX	201.87	2.66×10^{17}	223.3	225.4
Ultrafine spherical RDX	177.35	9.51×10^{14}	220.1	222.3

Table 3: Impact test results of raw RDX and ultrafine spherical RDX.

Sample	H_{50} (cm)	Standard
Raw RDX	21.5	0.07
Ultrafine spherical RDX	56.8	0.09

According to the activation energy and preexponential factors of different materials, the critical temperature of the thermal explosion was calculated by formulas (5) and (6), respectively [26]. The calculation results fare shown in Table 1.

$$T_{ei} = T_{e0} + b\beta_i + c\beta_i^2 + d\beta_i^3, \quad i = 1, 2, \ldots, 5, \tag{5}$$

$$T_b = \frac{E - \sqrt{E^2 - 4RET_{\varepsilon 0}}}{2R}. \tag{6}$$

The thermal decomposition kinetic parameters of the ultrafine spherical RDX and raw RDX are shown in Table 2. It could be seen that the apparent activation energy of the thermal decomposition of the ultrafine spherical RDX was lower than that of raw RDX and the frequency factors were also lower correspondingly. The critical temperature of the explosion of the ultrafine spherical RDX was slightly lower than that of raw RDX. The reason was as follows: when compared to raw RDX, the particle size of the RDX after refinement was significantly reduced. Besides, the particles with regular sphere shapes were obtained, which caused that the specific surface area to become larger and the heat transfer rate to become faster. Therefore, the activation energy was significantly decreased. The activation energy of spherical RDX prepared by spray drying by Shi Xiaofeng was 183.87 KJ/mol (the particle size was 0.5-5 μm), which was 18.5 KJ/mol lower than raw RDX; the result was consistent with this study. However, the activation energy of ultrafine spherical RDX obtained in this study was lower, which indicated that the ultrafine spherical RDX prepared in this study had smaller particle size, higher sphericity, and more uniform particle size distribution.

3.5. Impact Sensitivity Analysis. The results of the impact test are shown in Table 3. The ultrafine spherical RDX was prepared under the optimum conditions (drying temperature of 90°C, spray speed of 1 ml/min, and RDX mass fraction in solution of 4%).

As can be seen from Table 3, the H_{50} of the ultrafine spherical RDX was decreased by 35.3 cm compared to raw RDX, and the impact sensitivity was greatly reduced. The reason was as follows: the particle size of the ultrafine spherical RDX was smaller than that of raw RDX, and the crystal shape of the RDX particles obtained was a regular sphere. Moreover, the particle size was uniform and the dispersibility was fine. And the pore radius was much smaller than that of raw RDX. Therefore, the impact sensitivity of the ultrafine spherical RDX was much lower than that of raw RDX. The impact sensitivity of spherical RDX refined by spray drying by Shi Xiaofeng was also significantly lower than that of raw material RDX, and the H_{50} were 51.7 cm. This was consistent with the result of this study.

4. Conclusion

In this paper, ultrafine spherical RDX was prepared by the spray-drying method with low spraying speed and the optimum experimental conditions were concluded. The ultrafine spherical RDX prepared under the optimum experimental conditions had a narrow particle size distribution of 400-600 nm. The crystalline phases of the ultrafine spherical RDX and raw RDX were consistent, which indicated that the crystal structure of RDX was not changed during the process. The thermal decomposition apparent activation energy of ultrafine spherical RDX was slightly lower than that of raw RDX due to the fact that the particle size of the ultrafine spherical RDX was significantly lower than that of raw RDX. And the impact sensitivity of the ultrafine spherical RDX was much lower than that of raw RDX, which made the ultrafine spherical RDX more secure. Therefore, ultrafine spherical RDX can be used in propellants and insensitive booster explosives, and it has the potential to be used sustainably in energetic materials.

Data Availability

The data used to support the findings of this study are available from the corresponding author upon request.

Conflicts of Interest

The authors declare that they have no conflicts of interest.

Acknowledgments

This research work was financially supported by the Advantage Disciplines Climbing Plan and Graduate Education Innovation Project of Shanxi Province.

References

[1] A. T. Nielsen, S. L. Christian, D. W. Moore, R. D. Gilardi, and C. F. George, "Synthesis of 3,5,12-triazawurtzitanes (3,5,12-triazatetracyclo [5.3.1.12,6.04,9] dodecanes)," *Journal of Organic Chemistry*, vol. 52, no. 9, pp. 1656–1662, 2002.

[2] O. Bolton and A. J. Matzger, "Improved stability and smart-material functionality realized in an energetic cocrystal," *Angewandte Chemie*, vol. 50, no. 38, pp. 8960–8963, 2011.

[3] R. L. Simpson, P. A. Urtiew, D. L. Ornellas, G. L. Moody, K. J. Scribner, and D. M. Hoffman, "CL-20 performance exceeds

that of HMX and its sensitivity is moderate," *Propellants, Explosives, Pyrotechnics*, vol. 22, no. 5, pp. 249–255, 1997.

[4] G. Zeng, W. Pang, and J. Zhou, "Preparation and characterization of TATB based nanocomposites ☆," *Procedia Engineering*, vol. 102, pp. 610–614, 2015.

[5] T. M. Tillotson, A. E. Gash, R. L. Simpson, L. W. Hrubesh, J. H. Satcher Jr, and J. F. Poco, "Nanostructured energetic materials using sol–gel methodologies," *Journal of Non-Crystalline Solids*, vol. 285, no. 1-3, pp. 338–345, 2001.

[6] A. E. Gash, J. H. Satcher, R. L. Simpson, and B. J. Clapsaddle, "Nanostructured energetic materials with sol-gel methods," *MRS Proceedings*, vol. 800, 2003.

[7] U. Teipel, "Production of particles of explosives," *Propellants Explosives Pyrotechnics*, vol. 24, no. 3, pp. 134–139, 1999.

[8] H. Kasai, H. Oikawa, S. Okada, and H. Nakanishi, "Crystal growth of perylene microcrystals in the reprecipitation method," *Bulletin of the Chemical Society of Japan*, vol. 71, no. 11, pp. 2597–2601, 1998.

[9] Z. Yongxu, L. Dabin, and L. Chunxu, "Preparation and characterization of reticular nano-HMX," *Propellants Explosives Pyrotechnics*, vol. 30, no. 6, pp. 438–441, 2005.

[10] W. Yy, L. Yl, W. Jy, H. Ch, and A. Cw, "Preparation and characterization of nano-TATB," *Initiators & Pyrotechnics*, vol. 6, no. 8, pp. 794–800, 2013.

[11] G. Yang, F. Nie, H. Huang, L. Zhao, and W. Pang, "Preparation and characterization of nano-TATB explosive," *Propellants Explosives Pyrotechnics*, vol. 31, no. 5, pp. 390–394, 2006.

[12] V. Stepanov, L. N. Krasnoperov, I. B. Elkina, and X. Zhang, "Production of nanocrystalline RDX by rapid expansion of supercritical solutions," *Propellants Explosives Pyrotechnics*, vol. 30, no. 3, pp. 178–183, 2005.

[13] E. Reverchon, I. de Marco, and E. Torino, "Nanoparticles production by supercritical antisolvent precipitation: a general interpretation," *The Journal of Supercritical Fluids*, vol. 43, no. 1, pp. 126–138, 2007.

[14] B. M. Lee, D. S. Kim, Y. H. Lee et al., "Preparation of submicron-sized RDX particles by rapid expansion of solution using compressed liquid dimethyl ether," *Journal of Supercritical Fluids*, vol. 57, no. 3, pp. 251–258, 2011.

[15] X. L. Song, Y. Wang, L. X. Liu, C. W. An, J. Y. Wang, and J. L. Zhang, "Characterization of nano TATB fabricated by mechanical milling methodology," *Journal of Solid Rocket Technology*, vol. 40, no. 4, pp. 471–475, 2017.

[16] X. Guo, G. Ouyang, J. Liu et al., "Massive preparation of reduced-sensitivity nano CL-20 and its characterization," *Journal of Energetic Materials*, vol. 33, no. 1, pp. 24–33, 2014.

[17] D. Spitzer, C. Baras, M. R. Schäfer, F. Ciszek, and B. Siegert, "Continuous crystallization of submicrometer energetic compounds," *Propellants Explosives Pyrotechnics*, vol. 36, no. 1, pp. 65–74, 2010.

[18] V. Stepanov, V. Anglade, W. A. Balas Hummers, A. V. Bezmelnitsyn, and L. N. Krasnoperov, "Production and sensitivity evaluation of nanocrystalline RDX-based explosive compositions," *Propellants Explosives Pyrotechnics*, vol. 36, no. 3, pp. 240–246, 2011.

[19] H. Qiu, V. Stepanov, A. R. Di Stasio, T. Chou, and W. Y. Lee, "RDX-based nanocomposite microparticles for significantly reduced shock sensitivity," *Journal of Hazardous Materials*, vol. 185, no. 1, pp. 489–493, 2011.

[20] W. Ji, X. Li, and J. Wang, "Preparation and characterization of CL-20/EPDM by a crystal refinement and spray drying method," *Central European Journal of Energetic Materials*, vol. 12, no. 4, pp. 831–840, 2015.

[21] W. Jingyu, S. Xiaofeng, and L. Xiaodong, "Preparation and properties of RDX-nitrocellulose microspheres," *Central European Journal of Energetic Materials*, vol. 13, no. 4, pp. 871–881, 2016.

[22] B. Risse, D. Spitzer, D. Hassler et al., "Continuous formation of submicron energetic particles by the flash-evaporation technique," *Chemical Engineering Journal*, vol. 203, no. 5, pp. 158–165, 2012.

[23] J. W. Kim, M. S. Shin, J. K. Kim, H. S. Kim, and K. K. Koo, "Evaporation crystallization of RDX by ultrasonic spray," *Industrial & Engineering Chemistry Research*, vol. 50, no. 21, pp. 12186–12193, 2011.

[24] H. E. Kissinger, "Reaction kinetics in differential thermal analysis," *Analytical Chemistry*, vol. 29, no. 11, pp. 1702–1706, 1957.

[25] R. N. Rogers and G. W. Dauh, "Scanning calorimetric determination of vapor-phase kinetics data," *Analytical Chemistry*, vol. 45, no. 3, pp. 596–600, 2002.

[26] H. Wang, H. Zhang, R. Hu, E. Yao, and P. Guo, "Estimation of the critical rate of temperature rise for thermal explosion of nitrocellulose using non-isothermal DSC," *Journal of Thermal Analysis and Calorimetry*, vol. 115, no. 2, pp. 1099–1110, 2014.